Journal of Alloys and Compounds 527 (2012) 152–156

Contents lists available at SciVerse ScienceDirect

Journal of Alloys and Compounds

journal homepage: www.elsevier.com/locate/jallcom

Spectroscopic characteristics of 1.54 μm emission in Er/Yb:$LiNbO_3$ crystals tridoped with In^{3+} ions

Yannan Qian [a], Rui Wang [a,*], Chao Xu [a], Wei Xu [b], Xiaohong Wu [a], Chunhui Yang [a]

[a] Department of Chemistry, Harbin Institute of Technology, Harbin 150001, PR China
[b] Department of Physics, Harbin Institute of Technology, Harbin 150001, PR China

ARTICLE INFO

Article history:
Received 26 December 2011
Accepted 25 February 2012
Available online xxx

Keywords:
In/Er/Yb:$LiNbO_3$ crystal
Judd–Ofelt
Füchtbauer–Ladenburg
Fluorescence lifetime
Gain cross-section

ABSTRACT

A series of Er/Yb:$LiNbO_3$ crystals tridoped with x mol% In^{3+} ions (x = 1, 2 and 3 mol%) was grown by Czochralski technique. Under 980 nm excitation, the strongest intensity of 1.54 μm emission was observed for 2 mol% In^{3+}-tridoped Er/Yb:$LiNbO_3$ crystal. The UV–vis–infrared absorption spectra of In/Er/Yb:$LiNbO_3$ crystals were measured, and Judd–Ofelt (J–O) theory was carried out to predict the J–O intensity parameters (Ω_t), radiative lifetime τ_{rad} and fluorescence branching ratio β. The emission cross-section of the $^4I_{13/2} \rightarrow {}^4I_{15/2}$ transition of Er^{3+} ion was calculated by Füchtbauer–Ladenburg (F-L) method. The gain cross-section, estimated as a function of the population inversion ratio, allowed us to evaluate a potential laser performance of In/Er/Yb:$LiNbO_3$ crystal at 1.54 μm emission. The fluorescence lifetimes of the $^4I_{13/2} \rightarrow {}^4I_{15/2}$ transition in In/Er/Yb:$LiNbO_3$ crystals were measured.

© 2012 Elsevier B.V. All rights reserved.

1. Introduction

Owing to the development of wavelength division multiplexing (WDM) network systems of optical communication, Erbium-doped fiber amplifier (EDFA), a key device used in WDM system, has been gained significant attention [1,2]. Researches in this area based on Er^{3+}-doped silica glasses, polymers and crystals have been widely demonstrated [3–5]. Among these laser hosts, Er:$LiNbO_3$ crystal is of particular interest since the well-known versatile $LiNbO_3$ crystal, exhibiting electro-optic, piezo-electric and nonlinear optical physical properties, successfully combines with the amplifying and lasing characteristics of Er^{3+} ion [6–8]. The 1.54 μm emission arising from the $^4I_{13/2} \rightarrow {}^4I_{15/2}$ transition of Er^{3+} ion matches well with the third fiber-optics communication window [9]. The high efficiency of 1.54 μm emission could be obtained by the introduction of Yb^{3+} ion as a sensitizer [10,11].

The optical damage, inducing birefringence change and deforming the laser beams, still limits the practical nonlinear optical applications of $LiNbO_3$ crystal at high laser intensity. Advances in suppressing the optical damage effect have involved contributions from the optical damage resistant ions such as Mg^{2+}, Zn^{2+}, In^{3+}, Sc^{3+} and Hf^{4+} [12–15], which can improve the optical resistance of $LiNbO_3$ crystal by two orders of magnitude above their threshold concentration. The threshold concentrations are approximately 5.5 mol% for MgO [16], 7 mol% for ZnO [17] and 4 mol% for HfO_2 [18] in the congruent melt, which increase the difficulty in growing high quality crystals and further in obtaining waveguide-structure samples. For this reason, In_2O_3 should be investigated extensively due to its low threshold concentration (about 1.5 mol%) in $LiNbO_3$ [19]. Recently, a lot of researches on $LiNbO_3$ crystal doped with In^{3+} ions have been studied, such as the ultraviolet photo-refraction at 325 nm [20], the influence of In on nonvolatile holographic storage [21] and an enhanced 1.54 μm emission observed in Er:$LiNbO_3$ via codoping with In^{3+} ions [22]. However, none of reports on the laser performances of 1.54 μm emission in In/Er/Yb:$LiNbO_3$ tridoping system based on Judd–Ofelt theory and Füchtbauer–Ladenburg.

In this paper, In (1, 2 and 3 mol%)/Er (0.5 mol%)/Yb (0.5 mol%):$LiNbO_3$ crystals were grown by Czochralski technique. The spectroscopic characteristics of 1.54 μm emission in In/Er/Yb:$LiNbO_3$ crystals were investigated by the J–O theory, absorption and emission cross-section, gain cross-section spectra and the fluorescence lifetimes.

2. Experimental

$LiNbO_3$ crystals tridoped with Er_2O_3, Yb_2O_3 and In_2O_3 were grown by Czochralski technique using congruent melt composition ([Li]/[Nb] = 0.946). Both concentrations of Er^{3+} and Yb^{3+} ions were fixed at 0.5 mol% in the melt, while In^{3+} ion concentrations were changed as 1, 2 and 3 mol%. And the three crystals are named as In-1, In-2 and In-3, respectively. After all raw materials mixed for 24 h, the mixtures were heated at 750 °C for 2 h to remove CO_2, and then further heated up to 1150 °C for 2 h to form polycrystalline powder. The In/Er/Yb:$LiNbO_3$ crystals were grown under the optimum technology conditions as follows: an axial temperature gradient of 40–50 K/cm, the rotating rate of 10–25 rpm and the pulling rate of 0.5–2 mm/h. The grown crystals were polarized at 1200 °C with a current density of 5 mA/cm^2. The polarized crystals were cut into Y-plates ($X \times Y \times Z \approx 10\,mm \times 2\,mm \times 10\,mm$) with optically polished surfaces.

* Corresponding author. Tel.: +86 15846590861.
E-mail address: wangrui001@hit.edu.cn (R. Wang).

0925-8388/$ – see front matter © 2012 Elsevier B.V. All rights reserved.
doi:10.1016/j.jallcom.2012.02.160

Table 1
The Er content ($[Er^{3+}]/[Nb^{5+}]$ ratio) and the concentrations of Er^{3+} ion in the crystal measured from various In/Er/Yb:$LiNbO_3$ crystals.

Sample	In-1	In-2	In-3
$[Er^{3+}]/[Nb^{5+}]$ content in melt (mol%)	0.5	0.5	0.5
$[Er^{3+}]/[Nb^{5+}]$ content in crystal (mol%)	0.62	0.59	0.42
Er concentration in crystal ($\times 10^{20}$ cm^{-3})	1.171	1.114	0.982

The Er content ($[Er^{3+}]/[Nb^{5+}]$ ratio) in the crystal was determined by the inductively coupled plasma mass spectrometry (ICP-MS, Optima 7500 Series, Agilent Technologies Inc., Beijing). Table 1 illustrates the Er^{3+} content in the crystal and the concentrations of Er^{3+} ion in In-1, In-2 and In-3 crystals. The near infrared emission spectra were measured by the power-controllable 980 nm diode laser. All fluorescence emissions were recorded at the same geometry by using the spectrometer (Bruker optics 500IS/SM) equipped with a semiconductor cooled charge coupled device detector (DV440, Andor). The ultraviolet–visible (UV–vis)–infrared absorption spectra were measured with the CARY spectrophotometer in the range from 300 to 1650 nm. The fluorescence lifetimes of at 1.54 μm emission corresponding to $^4I_{13/2} \rightarrow {}^4I_{15/2}$ transition of Er^{3+} ion were measured by square-wave modulation of the electric current input to the 980 nm diode laser, and the induced time-resolved curves were recorded by a Yokogawa DLM 2054 digital phosphor oscilloscope. In order to minimize the measurement error, the thickness of the samples was further cut into 1 mm, which could reduce the luminescent path length.

3. Results and discussion

Fig. 1 displays the UV–vis–infrared absorption spectra of In-1, In-2 and In-3 crystals in the range from 300 to 1650 nm. The absorption bands centered at 368, 381, 410, 453, 492, 525, 550, 660 and 1540 nm are attributed to the transitions from the $^4I_{15/2}$ ground state to the $^4G_{9/2}$, $^4G_{11/2}$, $^2H_{9/2}$, $^4F_{3/2}$, $^4F_{7/2}$, $^2H_{11/2}$, $^4S_{3/2}$, $^4F_{9/2}$ and $^4I_{13/2}$ states of Er^{3+} ion. The 980 nm absorption bands arise from the overlapping of the $^4I_{15/2} \rightarrow {}^4I_{11/2}$ transition of Er^{3+} ion and the $^2F_{7/2} \rightarrow {}^2F_{5/2}$ transition of Yb^{3+} ion. The details on the theory and calculated procedure of Judd–Ofelt (J–O) have been reported in earlier Refs. [23–25]. The experimental transition strengths (f_{exp}), theoretical ones (f_{the}) and the corresponding root mean-square deviation (δ_{rms}) in In-1, In-2 and In-3 crystals are calculated and presented in Table 2. J–O intensity parameters Ω_t (t = 2, 4 and 6) of Er^{3+} ion in In/Er/Yb:$LiNbO_3$ crystals, derived from the electric dipole contributions of experimental transition strengths by a least-square fitting, are shown in Table 3. For comparative study, the J–O intensity parameters of some other reported Er^{3+}-doped crystals are also listed in Table 3. As illustrated in Table 2, the parameters δ_{rms} are 9.79×10^{-7}, 8.70×10^{-7} and 14.9×10^{-7}, respectively, for In-1, In-2 and In-3 crystals, which are larger than the previous calculated δ_{rms} in $LiNbO_3$ crystal single doped with Er^{3+} ion [26]. These results may be attributed to the poor scanning resolution in the optical absorption measurement. It can be seen from Table 3 that the trend of $\Omega_2 > \Omega_4 > \Omega_6$ for Er^{3+} ions is found in In/Er/Yb:$LiNbO_3$ tridoping system, suggesting that Er^{3+} ions are in a polarized environment. As the In^{3+} concentration increases the value of Ω_2 increases drastically, whereas the change of Ω_4 and Ω_6 parameters is comparative small. It is well known that Ω_2 is sensitive to the hypersensitive transitions $^4I_{15/2} \rightarrow {}^2H_{11/2}/{}^4G_{11/2}$ of Er^{3+} ions. A significant increase of Ω_2 caused by the increasing concentration of In^{3+} ions indicates that In^{3+} tridoping has much effect on hypersensitive transitions which are closely relate to the local polarization environment felt by rare-earth ions. Consequently, it is proposed that In_2O_3 tridoping could modify the Er^{3+}-site symmetries since the polarization characteristics of Er^{3+} ions are dependent on the Er^{3+}-site symmetries. In the case of the $^4I_{13/2} \rightarrow {}^4I_{15/2}$ transition of Er^{3+} ion corresponding to 1.54 μm emission, the S_{ed} line strength component is given by Carnall et al. [27]:

$$S_{ed} = 0.0195W_2 + 0.1173\Omega_4 + 1.4299\Omega_6 \quad (1)$$

where the numerical coefficients are the reduced matrix elements of the unit tensor operators, $U^{(t)}$, calculated in the intermediate-coupling approximation. According Eq. (1), the value of S_{ed} is mainly determined by Ω_6 parameters since its coefficient is two and one orders of magnitude greater than that of Ω_2 and Ω_4, respectively. An increase of Ω_6 is beneficial to enhance the emission bandwidth of 1.54 μm. Table 3 displays the values of Ω_6 in In-2 and In-3 crystals are larger than that in the other reported Er^{3+}-doped crystals, which suggest that Er/Yb:$LiNbO_3$ tridoped with In_2O_3 could achieve broadband and flat 1.54 μm emission. The spectroscopic quality factor X, defined by the ratio of the intensity parameter Ω_4 to Ω_6 ($X = \Omega_4/\Omega_6$), is an important predictor for stimulated emission in the laser active medium. As shown in Table 3, In-2 crystal has the largest spectroscopic quality factor X in the three In/Er/Yb:$LiNbO_3$ crystals. Moreover, the value of X in In-2 crystal is demonstrated to be almost the same as that in $NaLa(WO_4)_2$ crystal, and larger than that in Er:KLTN, Er:$YAlO_3$ and Er:$LuVO_4$ crystals, suggesting that In-2 crystal would be a promising candidate for laser medium at the wavelength of 1.54 μm.

The important radiative properties such as the fluorescence branching ratio β and the radiative lifetime τ_{rad} are calculated by using the J–O intensity parameters Ω_t (t = 2, 4 and 6) in In/Er/Yb:$LiNbO_3$ crystals and listed in Table 4. The corresponding formulas can be also found in Refs. [23–25]. The fluorescence branching ratio β of the $^4I_{11/2} \rightarrow {}^4I_{13/2}$ transition increases to 0.13998 for In-2 from 0.13782 for In-1, whereas decreases to 0.1124 for In-3 crystal. The enhancement of the fluorescence branching ratio β means the increased probability of the $^4I_{11/2} \rightarrow {}^4I_{13/2}$ radiative transfer, resulting in the increase in the 3 μm emission. This is an indication that In-2 crystal also could be applied in the 2.5–5.0 μm spectral region which is of great importance for medical applications, hazardous chemical detection, remote atmospheric sensing and pollution monitoring. On the other hand, an increased fluorescence branching ratios β of the $^4S_{3/2} \rightarrow {}^4I_{15/2}$ transition observed for In-3 crystal suggests the enhancement of the green emission. It has been reported that the green emission limits the amplification gain at 1.54 μm [32]. Therefore, there is a possibility that the 3 mol% In^{3+} tridoping would result in the reduction of the 1.54 μm emission in Er/Yb:$LiNbO_3$ crystal.

Fig. 2 presents the near infrared emission spectra of In-1, In-2 and In-3 crystals under 980 nm excitation. The near infrared emission centered at 1.54 μm is assigned to the $^4I_{13/2} \rightarrow {}^4I_{15/2}$ transition of Er^{3+} ion [33]. In comparison with In-1 crystal, the intensity of 1.54 μm emission is greatly enhanced by increasing the concentration of In^{3+} ions to 2 mol%. While the In^{3+} concentration is up

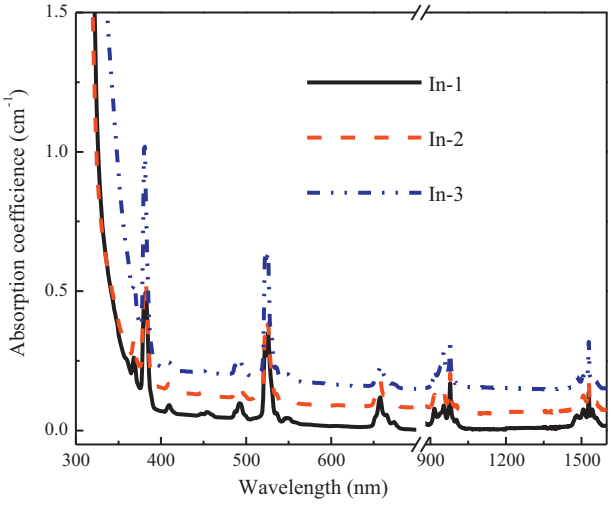

Fig. 1. The UV–vis–infrared absorption spectra of In-1, In-2 and In-3 crystals in the range from 300 to 1650 nm.

Table 2
The experimental transition strengths (f_{exp}) and theoretical ones (f_{the}), the corresponding root mean-square deviation (δ_{rms}). The units are 10^{-8} for all transition strengths and 10^{-7} for δ_{rms}.

Transition $^4I_{15/2}\rightarrow$	In-1		In-2		In-3	
	f_{exp}	f_{the}	f_{exp}	f_{the}	f_{exp}	f_{the}
$^4I_{13/2}$	218.8	218.7	204.9	208.3	299.9	300.9
$^4F_{9/2}$	350.7	342.6	327.6	323.7	377.5	384.1
$^4S_{3/2}$	42.95	56.25	38.71	52.12	67.13	91.09
$^2H_{11/2}$	1126.2	1019.1	1064.4	956.2	2304.2	2116.7
$^4F_{7/2}$	205.9	277.1	239.2	259.0	310.9	383.8
$^4F_{3,5/2}$	95.59	113.2	80.77	105.2	125.3	183.8
$^2H_{9/2}$	103.9	99.26	87.70	92.37	127.2	150.2
$^4G_{11/2}$	1827.8	2005.7	1720.5	1882.0	3894.7	4184.2
$^4G_{9/2}$	212.0	289.3	193.0	273.9	231.4	303.7
δ_{rms}	9.79		8.7		14.9	

Table 3
J–O intensity parameters Ω_t (t = 2, 4 and 6) and the spectroscopic quality factor X of Er^{3+} in In/Er/Yb:$LiNbO_3$ crystals and some other reported crystals.

Sample	J–O strength parameters, Ω_λ ($\times10^{-20}$ cm^2)			$X(\Omega_4/\Omega_6)$	Reference
	Ω_2	Ω_4	Ω_6		
In-1	7.23	3.14	1.42	2.21	This work
In-2	9.44	5.50	2.39	2.30	This work
In-3	24.9	5.38	4.19	1.28	This work
KLTN	3.13	1.16	1.49	0.80	[28]
$YAlO_3$	2.83	1.39	1.29	1.077	[29]
$LuVO_4$	13.3	3.04	1.60	1.90	[30]
$NaLa(WO_4)_2$	15.3	3.07	1.30	2.36	[31]

to 3 mol%, the 1.54 μm emission decreases, in agreement with the above prediction of the calculated fluorescence branching ratios β of $^4S_{3/2}\rightarrow{}^4I_{15/2}$.

The absorption cross-section (σ_{abs}) and emission cross-section (σ_{em}) of 1.54 μm emission in In/Er/Yb:$LiNbO_3$ crystals are calculated and displayed in Fig. 3. The absorption cross-section (σ_{abs}) can be obtained by Eq. (2) [34]. The emission cross-section (σ_{em}) could be used as a quantitative valuable factor to estimate the effectiveness of laser crystals, and the emission cross-section (σ_{em}) spectra can be derived using the Füchtbauer–Ladenburg Eq. (3) [35]:

$$\sigma_{abs}(\lambda) = 2.303\frac{OD(\lambda)}{Nd} \quad (2)$$

Table 4
Values of fluorescence branching ratios β and total radiative lifetimes τ_{rad} of excited states in In/Er/Yb:$LiNbO_3$ crystals.

Transition	In-1		In-2		In-3	
	β	τ_{rad} (τ_{meas})	β	τ_{rad} (τ_{meas})	β	τ_{rad} (τ_{meas})
$^4I_{13/2}\rightarrow{}^4I_{15/2}$	1	1414.3	1	1519.6	1	1339.9
$^4I_{11/2}\rightarrow{}^4I_{13/2}$	0.13782	909.3	0.13998	977.1	0.11833	748.0
$^4I_{15/2}$	0.86218		0.86002		0.88167	
$^4I_{9/2}\rightarrow{}^4I_{11/2}$	0.00426	519.6	0.00436	548.4	0.00522	662.2
$^4I_{13/2}$	0.1516		0.14839		0.20559	
$^4I_{15/2}$	0.84414		0.84724		0.78919	
$^4F_{9/2}\rightarrow{}^4I_{9/2}$	0.00868	70.7	0.00909	74.9	0.01173	84.5
$^4I_{11/2}$	0.02629		0.02583		0.0378	
$^4I_{13/2}$	0.04276		0.04283		0.04485	
$^4I_{15/2}$	0.92228		0.92225		0.90562	
$^4S_{3/2}\rightarrow{}^4F_{9/2}$	≈0	85.1	≈0	91.8	≈0	79.8
$^4I_{9/2}$	0.03789		0.03829		0.03304	
$^4I_{11/2}$	0.01905		0.0191		0.01846	
$^4I_{13/2}$	0.25656		0.25644		0.25804	
$^4I_{15/2}$	0.68619		0.68586		0.69015	
$^2H_{11/2}\rightarrow{}^4F_{9/2}$	0.00229	15.6	0.00227	16.5	0.00275	10.5
$^4I_{9/2}$	0.01055		0.01046		0.01079	
$^4I_{11/2}$	0.13865		0.14597		0.09433	
$^4I_{13/2}$	0.01559		0.01551		0.01218	
$^4I_{15/2}$	0.83292		0.8258		0.87995	
$^2H_{9/2}\rightarrow{}^4F_{7/2}$	0.00158	23.4	0.00155	24.4	0.00231	21.4
$^2H_{11/2}$	0.00471		0.00468		0.00429	
$^4F_{9/2}$	0.11205		0.11664		0.10264	
$^4I_{9/2}$	0.24929		0.25974		0.23192	
$^4I_{11/2}$	0.07991		0.07903		0.08684	
$^4I_{13/2}$	0.29405		0.28738		0.33112	
$^4I_{15/2}$	0.25841		0.25098		0.24089	

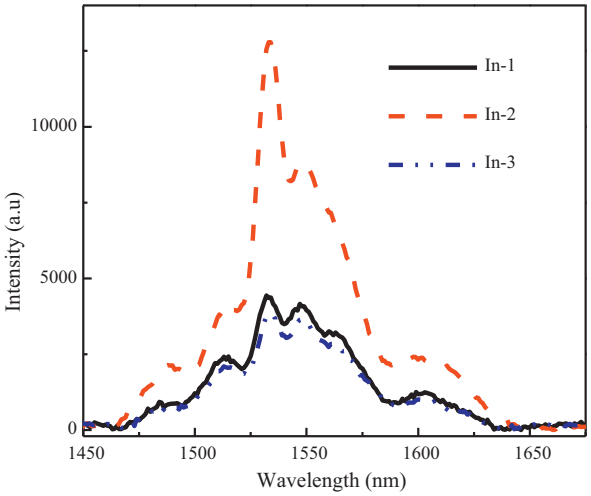

Fig. 2. The near infrared emission spectra of In/Er/Yb:$LiNbO_3$ crystals with various concentration of In^{3+} ions under 980 nm diode laser excitation.

$$\sigma_{em}(\lambda) = \frac{\lambda^5}{8\pi c n^2 \tau} \frac{I(\lambda)}{\int \lambda I(\lambda) d\lambda} \quad (3)$$

where λ is the absorption wavelength, OD (λ) is the optical density, N is the concentration of Er^{3+} ion in the crystal, d is the thickness of the sample in Eq. (2). In Eq. (3), λ is the emission wavelength, τ is the radiative lifetime, and n is the refractive index. As shown in Fig. 3, the maximum absorption cross-sections (σ_{abs}) at 1529 nm in In-1, In-2 and In-3 crystals are 1.26×10^{-20} cm^2, 1.14×10^{-20} cm^2 and 1.93×10^{-20} cm^2, respectively, and the maximum σ_{em} at 1534 nm are calculated to be 1.36×10^{-20} cm^2, 1.70×10^{-20} cm^2 and 1.33×10^{-20} cm^2, respectively. Further, the value of σ_{em} in In-2 is almost one order of magnitude higher than that in some other Er^{3+}-doped materials (for example σ_{em} at about 1550 nm is 0.59×10^{-20} cm^2 for Er:$LaGaO_3$ [36] and 0.5×10^{-20} cm^2 for Er:YAG [37]), and is comparable to the σ_{em} of 1.1×10^{-20} cm^2 for Er:$NaY(MoO_4)_2$ crystal [38]. In general, as a laser medium, the emission cross-section is as large as possible to provide high gain. From the view point of the practical application, the lasing action in Er:YAG crystal has been actualized at room temperature. Therefore, In-2 crystal could be attracted much attention to a promising candidate for commercial telecommunication application at the wavelength of 1.54 μm.

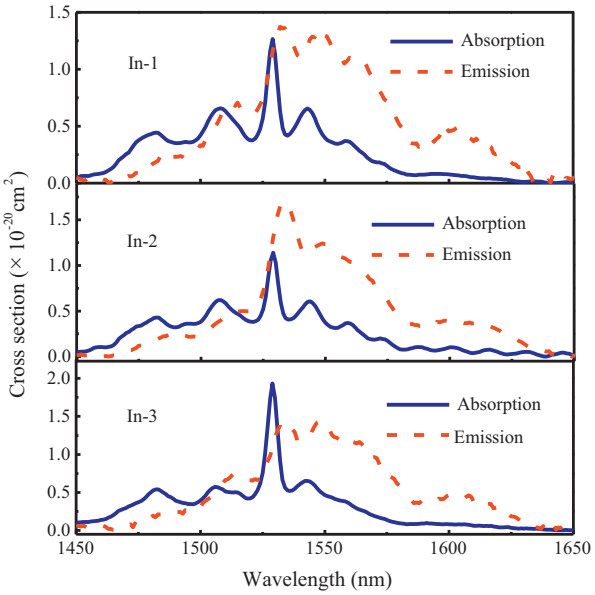

Fig. 3. The absorption and emission cross-section spectra of In/Er/Yb:$LiNbO_3$ crystals with various concentration of In^{3+} ions.

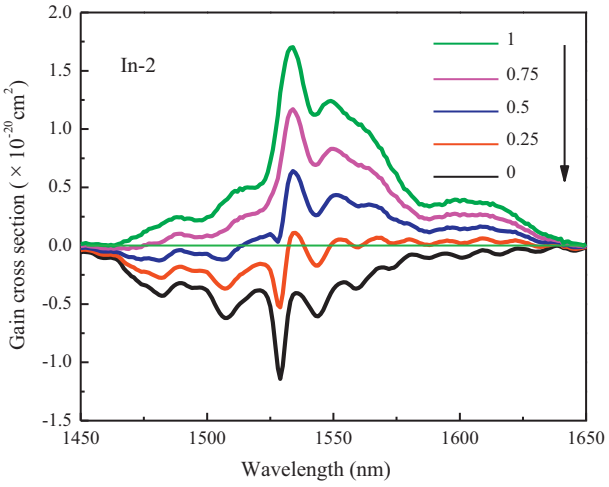

Fig. 4. Gain cross-section spectra for the $^4I_{13/2} \rightarrow {}^4I_{15/2}$ transitions as a function of the inverted population rate P.

Fig. 4 shows the gain cross-section of $^4I_{13/2} \rightarrow {}^4I_{15/2}$ transition in In-2 crystal as a function of P ranging from 0 to 1. Using the obtained absorption and emission cross-sections for In-2 crystal the gain cross-section is calculated according to [34]:

$$g(\lambda) = P\sigma_{em}(\lambda) - (1 - P)\sigma_{abs}(\lambda) \quad (4)$$

where P is the population inversion ratio of Er^{3+} ions, defined as the ratio of the electron population densities of $^4I_{13/2}$ to that of $^4I_{15/2}$ state. As P is equal to 0.5 in the gain cross-section spectrum, the value of g (λ) achieves a positive value at 1515 nm, and a relatively flat in the spectral range from 1551 to 1630 nm is observed, attributing to the C-band communication. With the inversion parameter P = 0.75, the gain cross-section reaches 1.18×10^{-20} cm^2 for In-2 crystal.

The fluorescence decay curves of the $^4I_{13/2} \rightarrow {}^4I_{15/2}$ transition in In/Er/Yb:$LiNbO_3$ crystals are shown in Fig. 5. The measured fluorescence lifetimes fitted by a single exponential behavior are obtained to be 3.55 ms, 3.33 ms and 3.30 ms for In-1, In-2 and In-3 crystals, respectively, which are longer than the calculated

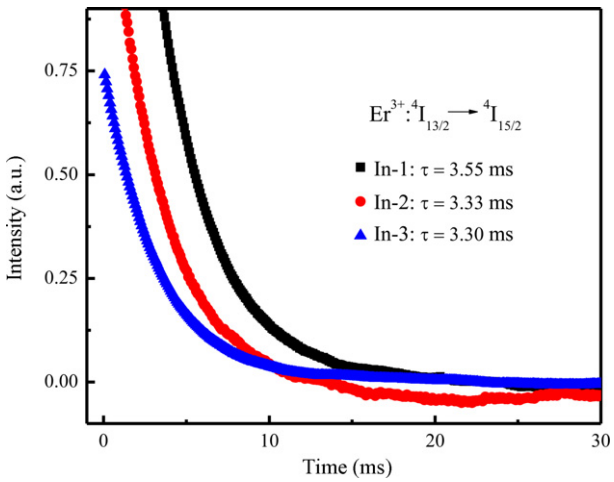

Fig. 5. The fluorescence decay curves of the $^4I_{13/2} \rightarrow {}^4I_{15/2}$ transition in In/Yb/Er:$LiNbO_3$ crystals.

radiative lifetimes (τ_{rad}) of $^4I_{13/2} \rightarrow {}^4I_{15/2}$ transition (τ_{rad} = 1.414 ms, 1.519 ms and 1.340 ms for In-1, In-2 and In-3 crystals, respectively). The discrepancy between the measured and calculated values is mainly caused by the radiation trapping effect, which has also been observed in many other Er^{3+}-doped hosts such as Er:LiLa(MoO_4)$_2$ [39] and Er:NaY(MoO_4)$_2$ [40]. Therefore, the thickness of the three crystals (1 mm) to suppress the radiation trapping effect may still be insufficient.

4. Conclusion

Spectroscopic properties of Er/Yb:$LiNbO_3$ crystals tridoped with various concentration of In^{3+} ions (1, 2 and 3 mol%) grown by the Czochralski technique are investigated and discussed. It is found that 2 mol% In^{3+} tridoping is the optimal doping concentration for the 1.54 μm emission under 980 nm excitation. Based on the calculated J–O intensity parameters Ω_t (t = 2, 4 and 6), the spectroscopic quality factor X ($X = \Omega_4/\Omega_6$) in In (2 mol%)/Er/Yb:$LiNbO_3$ crystal is larger than the other two In/Er/Yb:$LiNbO_3$ and some other reported Er^{3+}-doped crystals. The incorporation of In^{3+} ion has a strong effect on the Ω_2 parameters, suggesting that the Er^{3+}-site symmetries could be modified by In^{3+} ions. Besides the application in the 1.54 μm spectral region, In-2 crystal is predicted to be also suitable for the emission at 2.5–5.0 μm. The important parameters for estimating the potential laser action such as the absorption/emission cross-section and the gain cross-section spectra show that In/Er/Yb:$LiNbO_3$ crystals would be the potential laser operation at around 1.54 μm emission. Similar Er:LiLa(MoO_4)$_2$ and Er:NaY(MoO_4)$_2$, the measured fluorescence lifetimes of 1.54 μm emission are longer than the calculated radiative lifetimes (τ_{rad}). Some works on the exact measurement of the lifetime to avoid the radiation trapping effect should be further developed.

Acknowledgments

This work is financially supported by National Natural Science Foundation of China (10732100) and Natural Science Foundation of Heilongjiang Province of China (B200903). The authors also thank Prof. Z.G. Zhang for providing the measurement of the optical characteristics, who works in Department of Physics of Harbin Institute.

References

[1] J.A. Lázaro, M.A. Rebolledo, J.A. Vallés, IEEE J. Quantum Electron. 37 (2001) 1460.
[2] H.Y. Fan, G.N. Wang, K.F. Li, L.L. Hu, Solid State Commun. 150 (2010) 1101.
[3] S.Q. Xu, Z.M. Yang, S.X. Dai, J.H. Yang, L.L. Hu, Z.H. Jiang, J. Alloys Compd. 361 (2003) 313.
[4] D. Zhang, C. Chen, C.M. Chen, C.S. Ma, D.M. Zhang, Appl. Phys. Lett. 91 (2007) 161109.
[5] F. Liu, E. Ma, D.Q. Chen, Y.S. Wang, Y.L. Yu, P. Huang, J. Alloys Compd. 467 (2009) 317.
[6] J.B. Gruber, D.K. Sardar, R.M. Yow, B. Zandi, E.P. Kokanyan, Phys. Rev. B 69 (2004) 195103.
[7] L.H. Slooff, A. van Blaaderen, A. Polman, G.A. Hebbink, S.I. Klink, F.C.J.M. Van Veggel, D.N. Reinhoudt, J.W. Hofstraat, J. Appl. Phys. 91 (2002) 3955.
[8] J.J. Ju, T.Y. Kwon, S.I. Yun, M. Cha, H.J. Seo, Appl. Phys. Lett. 69 (1996) 1358.
[9] Y.M. Yang, Z.P. Yang, P.L. Li, X. Li, Q.L. Guo, B.J. Chen, Opt. Mater. 32 (2009) 133.
[10] J.C. Boyer, L.A. Cuccia, J.A. Capobianco, Nano Lett. 7 (2007) 847.
[11] J. Zheng, Y.L. Tao, W. Wang, L.Z. Zhang, Y.H. Zuo, C.H. Xue, Mater. Lett. 65 (2011) 860.
[12] T. Volk, M. Wöhlecke, N. Rubinina, N.V. Razumovski, F. Jermann, C. Fischer, R. Böwer, Appl. Phys. A 60 (1995) 217.
[13] T. Volk, N. Rubinina, M. Wöhlecke, J. Opt. Soc. Am. B 11 (1994) 1681.
[14] J.K. Yamamoto, T. Yanazaki, K. Yamagishi, Appl. Phys. Lett. 64 (1994) 3228.
[15] S.Q. Li, S.G. Liu, Y.F. Kong, D.L. Deng, G.Y. Gao, Y.B. Li, H.C. Gao, L. Zhang, Z.H. Hang, S.L. Chen, J.J. Xu, J. Phys.: Condens. Matter 18 (2006) 3527.
[16] N. Iyi, K. Kitamura, Y. Yajima, S. Kimura, Y. Furukawa, M. Sato, J. Solid State Chem. 118 (1995) 148.
[17] T.R. Volk, V.I. Pryalkin, N.M. Rubinina, Opt. Lett. 15 (1990) 996.
[18] E.P. Kokanyan, L. Razzari, I. Cristiani, V. Degiorgio, J.B. Gruber, Appl. Phys. Lett. 84 (2004) 1880.
[19] Y.F. Kong, J.K. Wen, H.F. Wang, Appl. Phys. Lett. 66 (1995) 280.
[20] F.F. Xin, G.Q. Zhang, F. Bo, H.F. Sun, Y.F. Kong, J.J. Xu, T. Volk, N.M. Rubinina, J. Appl. Phys. 107 (2010) 033113.
[21] B. Fu, G.Q. Zhang, X.M. Liu, Y. Shen, Q.J. Xu, Y.F. Kong, S.L. Chen, J.J. Xu, Acta Phys. Sin. 57 (2008) 2946.
[22] L. Sun, C.H. Yang, A.H. Li, Y.H. Xu, L.C. Zhao, J. Appl. Phys. 105 (2009) 043512.
[23] M.D. Shinn, W.A. Sibley, M.G. Drexhage, R.N. Brown, Phys. Rev. B 27 (1983) 6635.
[24] M.P. Hehlen, N.J. Cockroft, T.R. Gosnell, A.J. Bruce, Phys. Rev. B 56 (1997) 9302.
[25] H. Ping, D.Q. Chen, Y.L. Yu, Y.S. Wang, J. Alloys Compd. 490 (2010) 74.
[26] J. Amin, B. Dussardier, T. Schweizer, M. Hempstead, J. Lumin. 69 (1996) 17.
[27] W.T. Carnall, P.R. Fields, B.G. Wyboune, J. Chem. Phys. 42 (1965) 3797.
[28] L. Li, Z.X. Zhou, L. Feng, H. Li, Y. Wu, J. Alloys Compd. 509 (2011) 6457.
[29] Q. Donga, G.J. Zhao, D.H. Cao, J.Y. Chen, Y.C. Ding, J. Alloys Compd. 493 (2010) 661.
[30] R. Lisiecki, G.D. Dzik, P. Solarz, A. Strzęp, W.R. Romanowski, T. Łukasiewicz, Appl. Phys. B 101 (2010) 791.
[31] X.H. Gong, Y.J. Chen, Y.F. Lin, J.H. Huang, Z.D. Luo, Y.D. Huang, J. Appl. Phys. 108 (2010) 073524.
[32] D.L. Zhang, C. Wu, Q.Z. Yang, L. Sun, Y.H. Xu, E.Y.B. Pun, Appl. Phys. B 95 (2009) 335.
[33] S.Z. Lu, Q.H. Yang, B. Zhang, H.J. Zhang, Opt. Mater. 33 (2011) 746.
[34] J.H. Xie, Q. Zhang, Y.X. Zhuang, X.F. Liu, M.J. Guan, B. Zhu, R. Yang, J.R. Qiu, J. Alloys Compd. 509 (2011) 3032.
[35] U. Hömmerich, C. Hanley, E. Brown, S.B. Trivedi, J.M. Zavada, J. Alloys Compd. 488 (2009) 624.
[36] I. Sokólska, Appl. Phys. B 71 (2000) 157.
[37] H. Stange, K. Petermann, G. Huber, E.W. Duczynski, Appl. Phys. B 49 (1989) 269.
[38] X.A. Lu, Z.Y. You, J.F. Li, Z.J. Zhu, G.H. Jia, B.C. Wu, C.Y. Tu, J. Alloys Compd. 426 (2006) 352.
[39] X.Y. Huang, G.F. Wang, J. Alloys Compd. 475 (2009) 693.
[40] X.Z. Li, Z.B. Lin, L.Z. Zhang, G.F. Wang, J. Cryst. Growth 293 (2006) 157.